PHYSICAL REVIEW A **89**, 020702(R) (2014)

Photoassociation of ultracold LiRb* molecules: Observation of high efficiency and unitarity-limited rate saturation

Sourav Dutta,[1,*] John Lorenz,[1] Adeel Altaf,[1] D. S. Elliott,[1,2] and Yong P. Chen[1,2,†]
[1]*Department of Physics, Purdue University, West Lafayette, Indiana 47907, USA*
[2]*School of Electrical and Computer Engineering, Purdue University, West Lafayette, Indiana 47907, USA*

(Received 21 July 2013; published 19 February 2014)

We report the production of ultracold heteronuclear ^{7}Li^{85}Rb molecules in excited electronic states by photoassociation (PA) of ultracold ^{7}Li and ^{85}Rb atoms. PA is performed in a dual-species ^{7}Li-^{85}Rb magneto-optical trap (MOT) and the PA resonances are detected using trap loss spectroscopy. We identify several strong PA resonances below the Li $(2s\ ^2S_{1/2})$ + Rb $(5p\ ^2P_{3/2})$ asymptote and experimentally determine the long range C_6 dispersion coefficients. We find a molecule formation rate (P_{LiRb}) of $3.5 \times 10^7\ \mathrm{s}^{-1}$ and a PA rate coefficient (K_{PA}) of $1.3 \times 10^{-10}\ \mathrm{cm}^3/\mathrm{s}$, the highest among heteronuclear bi-alkali-metal molecules. At large PA laser intensity we observe the saturation of the PA rate coefficient (K_{PA}) close to the theoretical value at the unitarity limit.

DOI: 10.1103/PhysRevA.89.020702 PACS number(s): 34.50.−s, 33.20.−t, 37.10.Mn

Heteronuclear polar molecules have recently attracted enormous attention [1–17] owing to their ground state having a large electric dipole moment [16]. The long range anisotropic dipole-dipole interaction in such systems is the basis for a variety of applications including quantum computing [13], precision measurements [14], ultracold chemistry [2], and quantum simulations [15]. Heteronuclear bi-alkali-metal molecules (XY, where X and Y are two different alkali-metal-atom species), only a small subset of polar molecules, have received special attention mainly because the constituent alkali-metal atoms are easy to laser cool and can be easily associated to form molecules at ultracold temperatures. The two primary methods for production of heteronuclear bi-alkali-metal molecules have been magnetoassociation (MA), as in the case of KRb, NaK, and NaLi [1–4], and photoassociation (PA), as in the case of LiCs, RbCs, NaCs, KRb, and LiK [5–12]. Such molecules can be transferred to their absolute ground state where they have significant dipole moment, for example, by stimulated Raman adiabatic passage (STIRAP) [1,12]. There is considerable interest in other heteronuclear combinations either due to their higher dipole moments, different quantum statistics, or the possibility of finding simpler or more efficient methods for the production of ultracold molecules.

In this Rapid Communication we report a highly efficient production of ultracold ^{7}Li^{85}Rb molecules by PA (also see [18]). There is considerable interest in LiRb because the rovibronic ground state LiRb molecule is predicted to have a relatively high dipole moment of 4.1 D (exceeded only by LiCs and NaCs) [16], which makes it a strong candidate for many of the applications mentioned above. It is also interesting to note that bosonic ^{85}Rb, ^{87}Rb, and ^{7}Li, and the fermionic ^{6}Li are among the more commonly trapped alkali-metal-atomic species. This can make LiRb molecules readily available in both fermionic and bosonic forms (depending on the Li isotope chosen), broadening the range of physics that can be studied. We provide the first step towards the production of such ultracold LiRb molecules. In our experiment, the ^{7}Li^{85}Rb molecules are created in excited electronic states (denoted by LiRb*) by photoassociating ultracold ^{7}Li and ^{85}Rb atoms held in a dual-species magneto-optical trap (MOT). Contrary to previous expectation [19], we find very high LiRb* formation rate (P_{LiRb}) of $3.5 \times 10^7\ \mathrm{s}^{-1}$, which is promising for ultimately creating ultracold LiRb molecules in their rovibronic ground state. We also report a PA rate coefficient (K_{PA}) of $1.3 \times 10^{-10}\ \mathrm{cm}^3/\mathrm{s}$, the highest among heteronuclear bi-alkali-metal molecules. In addition, we observe the unitarity-limited saturation of K_{PA} at a value that is in agreement with the theory of Bohn and Julienne [20]. The observation of unitarity-limited saturation of K_{PA} has important implications, for example, in the observation of atom-molecule oscillations and coherent control (which often requires understanding the strongly driven regime) [20–25].

Our experiments are performed in a dual-species MOT. The details of the apparatus have been described elsewhere [26]. We use a conventional MOT for ^{7}Li and a dark MOT for ^{85}Rb which allows us to trap a large number of atoms with minimal losses from light-assisted interspecies collisions [26]. The spatial overlap of the two MOTs is monitored using a pair of CCD cameras placed orthogonal to each other and a good overlap is ensured for the PA experiments. The ^{85}Rb dark-MOT typically contains $N_{\mathrm{Rb}} \sim 1 \times 10^8$ ^{85}Rb atoms at a density (n_{Rb}) $\sim 4 \times 10^9\ \mathrm{cm}^{-3}$, with a majority of the ^{85}Rb atoms in the lower ($F = 2$) hyperfine level of the $5s\ ^2S_{1/2}$ state. The ^{7}Li MOT typically contains $N_{\mathrm{Li}} \sim 6 \times 10^7$ ^{7}Li atoms at a density (n_{Li}) $\sim 5 \times 10^9\ \mathrm{cm}^{-3}$, with a majority of the atoms in the upper ($F = 2$) hyperfine level of the $2s\ ^2S_{1/2}$ state. The atoms collide mainly along the ^{7}Li$\,(2s\,^2S_{1/2}, F = 2)$ + ^{85}Rb$\,(5s\,^2S_{1/2}, F = 2)$ channel. The fluorescence from both the MOTs is collected using a lens, separated using a dichroic mirror, and recorded on two separate photodiodes.

Light for the PA measurements is produced by a Ti:sapphire laser with a linewidth below 1 MHz, maximum output power of 480 mW, and maximum mode-hop-free scan of 20 GHz. The PA laser beam is collimated to a $1/e^2$ diameter of 0.85 mm, leading to a maximum available average intensity of about 85 W/cm^2. In this Rapid Communication we report PA resonances below the Li$\,(2s\,^2S_{1/2})$ + Rb$\,(5p\,^2P_{3/2})$ asymptote, i.e., near the D_2 line of Rb at 780 nm, while we have also recently observed PA resonances near the D_1 line

*sourav.dutta.mr@gmail.com
†yongchen@purdue.edu

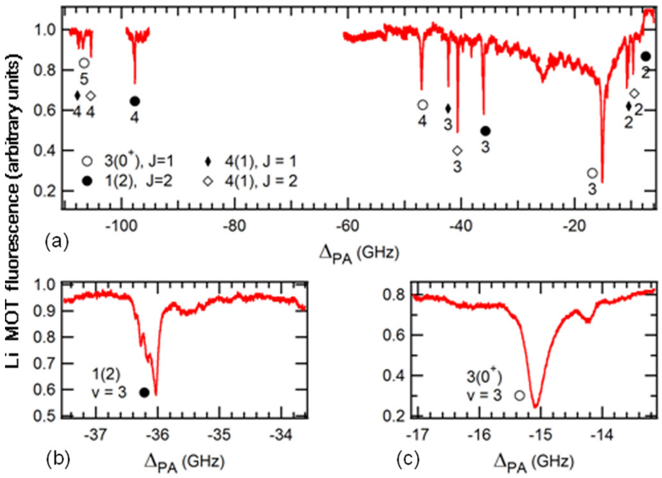

FIG. 1. (Color online) (a) PA spectra of LiRb obtained using trap loss spectroscopy. A reduction in the fluorescence of the Li MOT is observed whenever the PA laser is tuned through a LiRb* PA resonance. The open circles, filled circles, filled rhombus, and open rhombus indicate lines belonging to the $3(0^+)$, $1(2)$, $4(1)$ $J = 1$, and $4(1)$ $J = 2$ states, respectively, while the numbers indicate the vibrational level v measured from the dissociation limit (see text for details). (b) PA spectrum near the $v = 3$ level of the $1(2)$ state showing resolved hyperfine structure. (c) PA spectrum near the $v = 3$ level of the $3(0^+)$ state which is broad and leads to a 70% trap loss.

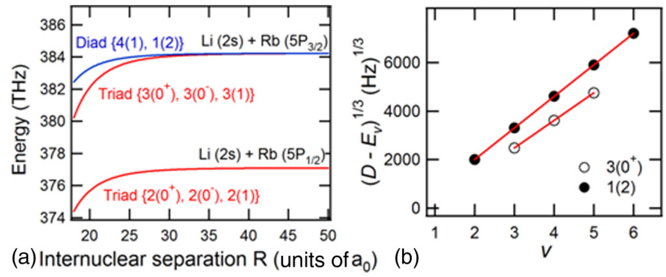

FIG. 2. (Color online) (a) The theoretical potential energy curves [28] for LiRb at large internuclear separations. Only curves near the Li $(2s)$ + Rb $(5p)$ asymptote are shown. (b) The fit to the LRB formula, Eq. (1), that is used to extract the C_6 coefficients from the experimentally measured PA line positions (to avoid clutter, only two representative states are shown).

of Rb at 795 nm [18]. PA resonances lead to the formation of LiRb* molecules which either spontaneously decay to LiRb molecules in the electronic ground state or to free Li and Rb atoms with high kinetic energies. Both mechanisms result in loss of the Li and Rb atoms from the MOT leading to a decrease in the MOT fluorescence. The formation of LiRb* molecules can thus be detected from this so called trap loss spectrum. In this work the signature of LiRb* PA resonances is detected through the trap loss in the Li MOT (the trap loss signal of the Rb MOT is complicated due to the presence of numerous Rb_2 PA resonances in addition to the LiRb PA resonances). We have also verified that the observed LiRb PA resonances are absent unless both the Li and Rb MOTs are simultaneously present.

A part of the experimentally observed PA spectrum below the Li $(2s\,^2S_{1/2})$ + Rb $(5p\,^2P_{3/2})$ asymptote is shown in Fig. 1. The detuning Δ_{PA} is measured with respect to the frequency ν_{res}(=384 232.157 GHz) of the Rb $(5s\,^2S_{1/2}, F = 2) \rightarrow$ Rb $(5p\,^2P_{3/2}, F' = 3)$ transition, i.e., $\Delta_{\text{PA}} = \nu_{\text{PA}} - \nu_{\text{res}}$, where ν_{PA} is the frequency of the PA laser. The detuning Δ_{PA} is thus a measure of the binding energy (E_B) of the respective vibrational levels. For the spectrum shown in Fig. 1(a), the frequency of the PA laser was scanned at 10 MHz/s (while the MOT loading time is $\sim$5 s) and the intensity of the PA beam was 70 W/cm^2. The full spectrum in Fig. 1(a) was obtained by stitching together many short 4 GHz scans. The absolute frequencies of the PA lines are accurate to $\pm$100 MHz, although the frequency resolution is much higher and hence the relative frequency measurements are more accurate. The narrowest PA lines have a linewidth of $\sim$33 MHz and we are able to resolve finer structures in the PA lines as shown in Fig. 1(b) (see Sec. S1 of the Supplementary Material [27] for a zoomed-in view of all observed PA resonances). Figure 1(c) shows the strongest PA line observed which corresponds to a LiRb* molecule production rate of 3.5×10^7 s^{-1}. We will elaborate on this particular PA line below but first discuss the assignment of the observed PA lines.

The theoretical potential energy curves at large internuclear separations (R) depend on the C_6 coefficients [28–30], an example of which is shown for LiRb in Fig. 2(a). In Hund's case (c) there are five electronic states asymptotic to the Li $(2s\,^2S_{1/2})$ + Rb $(5p\,^2P_{3/2})$ asymptote [28–33]. These are labeled $n(\Omega^\sigma)$, where Ω is the projection of the total electronic angular momentum on the internuclear axis, $\sigma = -/+$ (only for $\Omega = 0$) depending on whether or not the electronic wave function changes sign upon reflection at any plane containing the internuclear axis, and n is a number denoting the nth electronic state of a particular Ω^σ. The $3(0^+)$, $3(0^-)$, and $3(1)$ have very similar C_6 coefficients, are almost indistinguishable, and form a triad. The $4(1)$ and $1(2)$ have very similar C_6 coefficients, are almost indistinguishable, and form a diad. Only these five states are relevant for PA near the D_2 asymptote.

We have identified several vibrational levels belonging to the $3(0^+)$, $4(1)$, and $1(2)$ electronic states but did not observe the $3(0^-)$ and $3(1)$ states. For each vibrational level we observe at most two lines corresponding to two rotational levels (J). While it is true that s-wave collisions dominate in our system since the p-wave centrifugal barrier [$\sim$1.9 mK, estimated using $C_6 \sim 2500$ atomic units for the Li $(2s\,^2S_{1/2})$ + Rb $(5s^2S_{1/2})$ asymptote] is higher than the MOT temperatures ($\sim$1 mK and $\sim$200 μK for the Li and Rb MOTs, respectively), it does not provide a satisfactory explanation of why only up to two rotational levels are observed.

The selection rules for the electric dipole transitions are $\Delta\Omega = 0, \pm 1$, $\Delta J = 0, \pm 1$, $0^+ \leftrightarrow 0^+$, $0^- \leftrightarrow 0^-$, $J \geq \Omega$, $\Delta J = 0$ is not allowed if $\Omega = 0$ for both states and $J = 0 \rightarrow J = 0$ transitions are not allowed [10,31–33]. The Li and Rb atoms in the ground state collide along the $1(0^+)$, $1(0^-)$, or the $1(1)$ channels. Along with the assumption that only s-wave $(l = 0)$ collisions contribute, this leads to the following allowed levels of the photoassociated LiRb* molecule: 0^+ $(J = 0, 1, 2)$, 0^- $(J = 0, 1, 2)$, 1 $(J = 1, 2)$, and 2 $(J = 2)$. However, for reasons that remain to be understood, we observe at most two of the allowed rotational levels. For the $\Omega = 0^+$ state we observe only one J and hence cannot accurately assign the value of J.

TABLE I. The values of $-\Delta_{\mathrm{PA}}$ (in GHz) for which PA lines are observed.

State	$v = 2$	$v = 3$	$v = 4$	$v = 5$	$v = 6$
$3(0^+)$, $J = 1$		15.08	47.03	106.76	
$1(2)$, $J = 2$	7.91	36.06	97.61	205.52	373.07
$4(1)$, $J = 2$	9.62	40.69	105.36		
$4(1)$, $J = 1$	10.75	42.35	107.50		

On the other hand, the width and the hyperfine structure of the observed PA lines allow us to make an educated guess for J and also of Ω. We assign the relatively wide ($\sim$250 MHz) PA lines to $3(0^+)$, $J = 1$ since (i) the linewidth of $3(0^+)$ resonances are expected to be large since the $3(0^+)$ state, which correlates to the $b\,^3\Pi$-$A\,^1\Sigma^+$ complex at smaller internuclear distances, could undergo predissociation [33] due to the avoided crossing [34] between the $b\,^3\Pi$ and $A\,^1\Sigma^+$ states, (ii) they are expected to have no hyperfine structure, and (iii) they fit the expected line positions of the triad potential quite well as discussed in detail below. We assign the lines with multiple resolved hyperfine splitting to $1(2)$, $J = 2$ since (i) the hyperfine splitting is expected to be the largest for these lines [35] and (ii) they fit the diad potential quite well. We assign the other lines to the $J = 1$ and $J = 2$ levels of the $4(1)$ state based on the agreement with the expected rotational constant.

For the $3(0^+)$ state we prefer assigning $J = 1$ instead of $J = 0$ or $J = 2$ because there are at least twice as many allowed PA transitions from the $1(0^+)$, $1(0^-)$, and $1(1)$ collision channels that lead to the formation of $J = 1$ LiRb* molecules compared to $J = 0$ or $J = 2$ LiRb* molecules. In Table I we report all the observed PA lines along with their assignments. For levels with hyperfine structure, the position of the strongest line is reported. We note that the identification of the diad and triad potentials and the derived C_6 coefficients are expected to be quite accurate despite some uncertainties in the assignment of the angular momentum quantum numbers such as J.

To extract the C_6 coefficients we use the LeRoy-Bernstein (LRB) formula [36]:

$$D - E_v = A_6(v - v_D)^3, \tag{1}$$

where v is the vibrational quantum number measured from the dissociation limit (i.e., measured such that $v = 1$ is the least bound state), v_D $(0 < v_D < 1)$ is the vibrational quantum number at dissociation, $-(D - E_v)$ is the (negative) binding energy E_B, D is the (positive) dissociation energy, E_v is the (positive) energy of the vth vibrational level, and $A_6 = 16\sqrt{2}\pi^3\hbar^3/\{[B(2/3,1/2)]^3\mu^{3/2}C_6^{1/2}\}$, with μ being the reduced mass of ^{7}Li^{85}Rb and B being the Beta function $[B(2/3,1/2) = 2.5871]$. Note that $(D - E_v) - E_{\mathrm{rot}} = -h\Delta_{\mathrm{PA}}$ is experimentally measured, where $E_{\mathrm{rot}} = B_v[J(J+1) - \Omega^2]$ is the rotational energy, and B_v is the rotational constant.

For each Ω state we first assign the vibrational quantum number (v) and then plot $(-h\Delta_{\mathrm{PA}})^{1/3} \approx (D - E_v)^{1/3}$ against v, neglecting the small contribution from E_{rot}. We then derive the values of v_D and A_6 (and hence C_6) from a fit to Eq. (1), an example of which is shown in Fig. 2(b). Accounting for E_{rot}, which is small ($135 \leqslant B_v \leqslant 515$ MHz), does not change these values significantly (see Sec. S2 in Ref. [27]) and the

TABLE II. The values of C_6 coefficients (in atomic units) for the Li ($2s\,^2S_{1/2}$) + Rb ($5p\,^2P_{3/2}$) asymptote measured experimentally in this work, and a comparison with three different theoretical predictions. The numbers in parentheses indicate the uncertainties in the experimental determination. The experimentally determined values of v_D are also included.

	This work				
	v_D	C_6	C_6 [28]	C_6 [29]	C_6 [30]
$3(0^+)$	0.80	20 160 (950)	20 670	24 980	26 744
$1(2)$	0.40	9 235 (490)	9 205	11 308	9 431
$4(1)$	0.24	10 190 (420)	9 205	11 308	9 431

C_6 coefficients are within the quoted uncertainties even if the rotational assignment (J) is changed by ± 1. We compare the experimentally determined C_6 coefficients with the theoretical values available (Table II) and generally find good agreement with Ref. [28] and reasonable agreement with others.

We now turn our attention to the strongest PA lines at $\Delta_{\mathrm{PA}} = -15.08$ GHz ($\nu_{\mathrm{PA}} = 384\,217.07$ GHz) for which we observe 70% losses in the Li MOT. In Fig. 3(a) we show the time evolution of the number of atoms in the Li MOT when the resonant PA beam, with average intensity = 74 W/cm^2, is turned on at $t = 0$ (see Sec. S3 in Ref. [27]). From the initial slope of the curve we determine that 3.5×10^7 Li

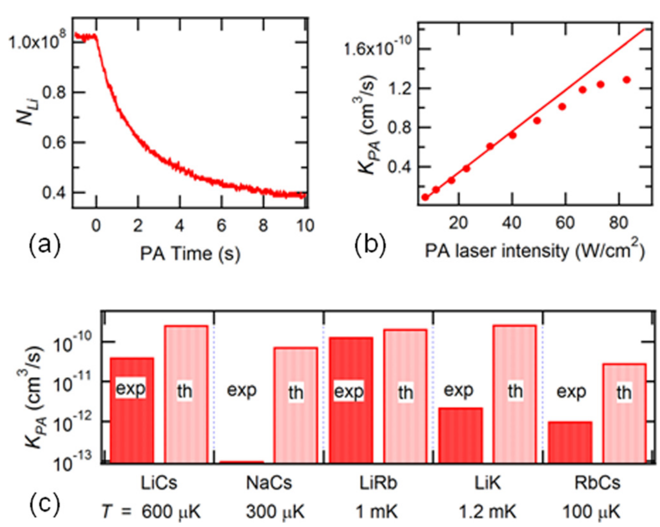

FIG. 3. (Color online) (a) The evolution of the atom number N_{Li} in the Li MOT when the on resonance PA light [$\nu_{\mathrm{PA}} = 384\,217.07$ GHz, the resonance shown in Fig. 1(c)] is turned on at $t = 0$. The LiRb* production rate (P_{LiRb}) is estimated from the slope near $t = 0$. (b) The PA rate coefficient (K_{PA}) as a function of the average PA laser intensity. The rate starts to saturate beyond 60 W/cm^2. The solid line is a linear fit of K_{PA} in the low-intensity regime with a slope 2×10^{-12} (cm^3/s)/(W/cm^2). (c) Comparison of PA rate coefficient K_{PA} of different polar molecules. The left (dark color, expt.) bars denote the maximum experimentally observed values of K_{PA} while the right (light color, theor.) bars denote the theoretical values at the unitarity limit at the temperatures indicated. Even at a relatively high temperature, the K_{PA} for LiRb is the highest and is close to the theoretical prediction of the unitarity limit.

atoms are lost per second. This implies a LiRb* production rate (P_{LiRb}) of 3.5×10^7 s^{-1}, which is among the highest observed for heteronuclear bi-alkali-metal molecules. Since the Rb MOT is larger than the Li MOT, the PA rate coefficient K_{PA} is simply given by $K_{\mathrm{PA}} = P_{\mathrm{LiRb}}/(n_{\mathrm{Rb}} N_{\mathrm{Li}})$. Using the typical values of N_{Li} and n_{Rb}, the maximum value that we obtain is $K_{\mathrm{PA}} = 1.3 \times 10^{-10}$ cm^3/s. The value of K_{PA} is accurate to within 50%, the major uncertainty coming from the determination of n_{Rb} (note that the uncertainties in the measurement of N_{Li} cancel out). We also observe the saturation of P_{LiRb} and hence K_{PA}, for PA laser intensities exceeding 60 W/cm^2 [Fig. 3(b)]. The saturated value of K_{PA} is estimated to be around $1.3(7) \times 10^{-10}$ cm^3/s. This value can be compared to the predicted theoretical value at the unitarity limit where the scattering matrix element becomes unity [20,24,32]:

$$K_{\mathrm{PA,unitarity}} = \pi \upsilon_{\mathrm{rel}}/k^2 = \hbar^2 \sqrt{2\pi/\mu^3 k_B T}$$
$$= 2.1 \times 10^{-10}\ \mathrm{cm}^3/\mathrm{s},$$

where $\upsilon_{\mathrm{rel}} = \sqrt{8 k_B T/\pi \mu}$ is the average relative velocity of the atoms, $k = \sqrt{2\mu k_B T/\hbar^2}$, μ is the reduced mass, and $T = 1$ mK is the temperature of the Li atoms. Given the uncertainty in the values of n_{Rb} and T, we consider that the agreement between experiment and theory is fairly good. We note that we performed a similar analysis for PA of $^{85}Rb_2$ and found good agreement with theory [20] and with previous experimental reports.

In Fig. 3(c) we plot the maximum observed K_{PA} values for different polar molecules along with the theoretical values at the unitarity limit [20]. It is seen that the experimentally observed K_{PA} value for LiRb is higher than all other species so far and approaches the unitarity limit. We note that K_{PA} can be further increased by lowering T. It is also seen that for most other species the experimental maximum values differ substantially from the values at the unitarity limit. Moreover, the measured K_{PA} values for LiCs [37] and NaCs [38] have large error bars and are only accurate within a factor of 10. The error bars are large in those measurements because the measurements were performed using resonance enhanced multiphoton ionization (REMPI) for which it is difficult to calibrate the ionization, ion collection, and detection efficiencies. PA induced trap loss was used to measure PA rates in RbCs [9] and LiK [10] but the rates were significantly lower. In this regard, LiRb is a welcome exception with very high PA rate and the observation of PA-induced trap loss allows relatively precise determination of the PA rate coefficient K_{PA}. We note that high PA rate (though lower than that observed here) is also observed for PA near the Li $(2s\,^2S_{1/2})$ + Rb $(5p\,^2P_{1/2})$ asymptote [18].

We also note that we observe a very high LiRb* molecule production rate (P_{LiRb}) of 3.5×10^7 s^{-1}. Assuming that a small fraction of the LiRb* molecules would spontaneously decay to electronic ground state LiRb molecules, this amounts to a substantial production rate of LiRb molecules in the electronic ground state (see Sec. S4 in Ref. [27] for discussions on the prospects and schemes to create ground state LiRb molecules). Detection of such ground state molecules using REMPI, guided by our previous spectroscopy work [39], is currently being pursued.

In conclusion, we have produced ultracold LiRb* molecules by photoassociation and derived the C_6 dispersion coefficients for the Li $(2s\,^2S_{1/2})$ + Rb $(5p\,^2P_{3/2})$ asymptote. We find unexpectedly high LiRb* molecule production rate of 3.5×10^7 s^{-1}. We observe a PA rate coefficient (K_{PA}) of 1.3×10^{-10} cm^3/s, highest among heteronuclear bi-alkali-metal molecules, and report the PA laser intensity driven saturation of K_{PA} at a value close to the unitarity limit. We note that PA could lead to formation of LiRb molecules in the deeply bound vibrational levels of the ground electronic $X\ ^1\Sigma^+$ state. These can then be transferred to the $X\ ^1\Sigma^+$ ($v'' = 0$) state by techniques such as STIRAP [1,12] or optical pumping [40].

We thank Olivier Dulieu, Jesús Pérez-Ríos, and Michael Bellos for helpful discussions and feedback. S.D. acknowledges financial support from Purdue University in the form of the Bilsland Dissertation Fellowship. Support during early stages of this work by the NSF (CCF-0829918), and through an equipment grant from the ARO (W911NF-10-1-0243), are gratefully acknowledged.

[1] K.-K. Ni, S. Ospelkaus, M. H. G. de Miranda, A. Pe'er, B. Neyenhuis, J. J. Zirbel, S. Kotochigova, P. S. Julienne, D. S. Jin, and J. Ye, Science **322**, 231 (2008).

[2] S. Ospelkaus, K.-K. Ni, D. Wang, M. H. G. de Miranda, B. Neyenhuis, G. Quéméner, P. S. Julienne, J. L. Bohn, D. S. Jin, and J. Ye, Science **327**, 853 (2010).

[3] C.-H. Wu, J. W. Park, P. Ahmadi, S. Will, and M. W. Zwierlein, Phys. Rev. Lett. **109**, 085301 (2012).

[4] M.-S. Heo, T. T. Wang, C. A. Christensen, T. M. Rvachov, D. A. Cotta, J.-H. Choi, Y.-R. Lee, and W. Ketterle, Phys. Rev. A **86**, 021602(R) (2012).

[5] J. Deiglmayr, A. Grochola, M. Repp, K. Mörtlbauer, C. Glück, J. Lange, O. Dulieu, R. Wester, and M. Weidemüller, Phys. Rev. Lett. **101**, 133004 (2008).

[6] J. M. Sage, S. Sainis, T. Bergeman, and D. DeMille, Phys. Rev. Lett. **94**, 203001 (2005).

[7] P. Zabawa, A. Wakim, M. Haruza, and N. P. Bigelow, Phys. Rev. A **84**, 061401(R) (2011).

[8] D. Wang, J. Qi, M. F. Stone, O. Nikolayeva, H. Wang, B. Hattaway, S. D. Gensemer, P. L. Gould, E. E. Eyler, and W. C. Stwalley, Phys. Rev. Lett. **93**, 243005 (2004).

[9] A. J. Kerman, J. M. Sage, S. Sainis, T. Bergeman, and D. DeMille, Phys. Rev. Lett. **92**, 033004 (2004).

[10] A. Ridinger, S. Chaudhuri, T. Salez, D. R. Fernandes, N. Bouloufa, O. Dulieu, C. Salomon, and F. Chevy, Europhys. Lett. **96**, 33001 (2011).

[11] J. Ulmanis, J. Deiglmayr, M. Repp, R. Wester, and M. Weidemüller, Chem. Rev. **112**, 4890 (2012).

[12] K. Aikawa, D. Akamatsu, M. Hayashi, K. Oasa, J. Kobayashi, P. Naidon, T. Kishimoto, M. Ueda, and S. Inouye, Phys. Rev. Lett. **105**, 203001 (2010).

[13] D. DeMille, Phys. Rev. Lett. **88**, 067901 (2002).

[14] E. R. Hudson, H. J. Lewandowski, B. C. Sawyer, and J. Ye, Phys. Rev. Lett. **96**, 143004 (2006).

[15] M. A. Baranov, M. Dalmonte, G. Pupillo, and P. Zoller, Chem. Rev. **112**, 5012 (2012).

[16] M. Aymar and O. Dulieu, J. Chem. Phys. **122**, 204302 (2005).

[17] R. V. Krems, W. C. Stwalley, and B. Friedrich, *Cold Molecules: Theory, Experiment, Applications* (CRC, Taylor and Francis, New York, 2009).

[18] S. Dutta, D. S. Elliott, and Y. P. Chen, Europhys. Lett. **104**, 63001 (2013).

[19] H. Wang and W. C. Stwalley, J. Chem. Phys. **108**, 5767 (1998).

[20] J. L. Bohn and P. S. Julienne, Phys. Rev. A **60**, 414 (1999).

[21] I. D. Prodan, M. Pichler, M. Junker, R. G. Hulet, and J. L. Bohn, Phys. Rev. Lett. **91**, 080402 (2003).

[22] C. McKenzie, J. Hecker Denschlag, H. Häffner, A. Browaeys, L. E. E. de Araujo, F. K. Fatemi, K. M. Jones, J. E. Simsarian, D. Cho, A. Simoni, E. Tiesinga, P. S. Julienne, K. Helmerson, P. D. Lett, S. L. Rolston, and W. D. Phillips, Phys. Rev. Lett. **88**, 120403 (2002).

[23] U. Schlöder, C. Silber, T. Deuschle, and C. Zimmermann, Phys. Rev. A **66**, 061403(R) (2002).

[24] P. Pellegrini and R. Côté, New J. Phys. **11**, 055047 (2009).

[25] M. Yan, B. J. DeSalvo, Y. Huang, P. Naidon, and T. C. Killian, Phys. Rev. Lett. **111**, 150402 (2013).

[26] S. Dutta, A. Altaf, J. Lorenz, D. S. Elliott, and Y. P. Chen, arXiv:1306.5196.

[27] See Supplemental Material at http://link.aps.org/supplemental/10.1103/PhysRevA.89.020702 for zoomed in view of all PA lines, approximations made in calculating C_6, additional figures on PA rates, and discussions on ground state molecule formation.

[28] M. Movre and R. Beuc, Phys. Rev. A **31**, 2957 (1985).

[29] B. Bussery, Y. Achkar, and M. Aubert-Frécon, Chem. Phys. **116**, 319 (1987).

[30] M. Marinescu and H. R. Sadeghpour, Phys. Rev. A **59**, 390 (1999).

[31] G. Herzberg, *Molecular Spectra and Molecular Structure I: Spectra of Diatomic Molecules* (Van Nostrand, Princeton, NJ, 1961).

[32] K. M. Jones, E. Tiesinga, P. D. Lett, and P. S. Julienne, Rev. Mod. Phys. **78**, 483 (2006).

[33] W. C. Stwalley, M. Bellos, R. Carollo, J. Banerjee, and M. Bermudez, Mol. Phys. **110**, 1739 (2012).

[34] M. Korek, G. Younes, and S. AL-Shawa, J. Mol. Struct.: Theochem. **899**, 25 (2009).

[35] A. Grochola, A. Pashov, J. Deiglmayr, M. Repp, E. Tiemann, R. Wester, and M. Weidemüller, J. Chem. Phys. **131**, 054304 (2009).

[36] R. J. LeRoy and R. B. Bernstein, J. Chem. Phys. **52**, 3869 (1970).

[37] J. Deiglmayr, P. Pellegrini, A. Grochola, M. Repp, R. Côté, O. Dulieu, R. Wester, and M. Weidemüller, New J. Phys. **11**, 055034 (2009).

[38] C. Haimberger, J. Kleinert, O. Dulieu, and N. P. Bigelow, J. Phys. B: At. Mol. Opt. Phys. **39**, S957 (2006).

[39] S. Dutta, A. Altaf, D. S. Elliott, and Y. P. Chen, Chem. Phys. Lett. **511**, 7 (2011).

[40] I. Manai, R. Horchani, H. Lignier, P. Pillet, D. Comparat, A. Fioretti, and M. Allegrini, Phys. Rev. Lett. **109**, 183001 (2012).